Structural and kinetic basis for heightened immunogenicity of T cell vaccines

Ji-Li Chen,[1] Guillaume Stewart-Jones,[2] Giovanna Bossi,[3] Nikolai M. Lissin,[4] Linda Wooldridge,[5] Ed Man Lik Choi,[1] Gerhard Held,[6] P. Rod Dunbar,[1] Robert M. Esnouf,[2] Malkit Sami,[4] Jonathan M. Boulter,[4] Pierre Rizkallah,[7] Christoph Renner,[6] Andrew Sewell,[5] P. Anton van der Merwe,[3] Bent K. Jakobsen,[4] Gillian Griffiths,[3] E. Yvonne Jones,[2] and Vincenzo Cerundolo[1]

[1]Tumour Immunology Unit, Weatherall Institute of Molecular Medicine, University of Oxford, John Radcliffe Hospital, Oxford, UK, OX3 9DS
[2]Division of Structural Biology, Wellcome Trust Centre for Human Genetics, University of Oxford, Oxford, UK, OX3 7BN
[3]Sir William Dunn School of Pathology, University of Oxford, Oxford, UK, OX1 3RE
[4]Avidex Ltd., Abingdon, Oxon, UK, OX14 4RX
[5]T Cell Modulation Group, Peter Medawar Building, University of Oxford, Oxford, UK, OX1 3SY
[6]I. Med. Klinik, Saarland, University Medical School, 66421 Homburg/Saar, Germany
[7]CCLRC Daresbury Laboratory, Warrington, Cheshire, UK, WA4 4AD

Analogue peptides with enhanced binding affinity to major histocompatibility class (MHC) I molecules are currently being used in cancer patients to elicit stronger T cell responses. However, it remains unclear as to how alterations of anchor residues may affect T cell receptor (TCR) recognition. We correlate functional, thermodynamic, and structural parameters of TCR–peptide–MHC binding and demonstrate the effect of anchor residue modifications of the human histocompatibility leukocyte antigens (HLA)–A2 tumor epitope NY–ESO-$1_{157–165}$–SLLMWITQC on TCR recognition. The crystal structure of the wild-type peptide complexed with a specific TCR shows that TCR binding centers on two prominent, sequential, peptide sidechains, methionine–tryptophan. Cysteine-to-valine substitution at peptide position 9, while optimizing peptide binding to the MHC, repositions the peptide main chain and generates subtly enhanced interactions between the analogue peptide and the TCR. Binding analyses confirm tighter binding of the analogue peptide to HLA–A2 and improved soluble TCR binding. Recognition of analogue peptide stimulates faster polarization of lytic granules to the immunological synapse, reduces dependence on CD8 binding, and induces greater numbers of cross-reactive cytotoxic T lymphocyte to SLLMWITQC. These results provide important insights into heightened immunogenicity of analogue peptides and highlight the importance of incorporating structural data into the process of rational optimization of superagonist peptides for clinical trials.

CORRESPONDENCE
Vincenzo Cerundolo:
vincenzo.cerundolo@imm.ox.ac.uk

Abbreviations used: CDR, complementarity determining region; MW, methionine–tryptophan; pMHC, peptide–MHC.

A major challenge for the design of cancer vaccines is that natural tumor antigens elicit relatively weak T cell responses. One approach currently being investigated is the optimization of the MHC class I anchor residues in tumor epitopes to enhance binding of the peptide to the MHC class I molecule. Vaccination of cancer patients with this type of peptide analogue has resulted in larger antigen-specific CTL expansions than vaccination with wild-type peptides (1), indicating that the use of peptide analogs should be considered for future clinical trials. However, questions remain as to how alterations of anchor residues, while enhancing the peptide–MHC (pMHC) class I interaction, may affect TCR recognition.

The three-dimensional structures underlying TCR recognition have important implications for the design of molecular vaccines (2, 3). Structural studies have established the molecular characteristics determining peptide binding to MHC class I molecules (4). By comparison, relatively few structures of TCR–pMHC complexes have been solved (5), a particular problem hav-

Ji-Li Chen and Guillaume Stewart-Jones contributed equally to this work.

The online version of this article contains supplemental material.

ing being production of stable, soluble TCRs suitable for crystallization. One, potentially generic, solution to this problem is to engineer a novel interchain disulfide bond into the interface between the TCR constant domains (6), an approach exploited in the work reported here. Previous studies have compared the structures of pMHC complexes with those of altered peptide ligands, for example (7–9). These comparisons have demonstrated that substitutions of anchor residues can cause slight structural alterations that may indirectly impact on TCR recognition. Whereas the structural effects of changing surface exposed peptide residues have been studied directly in TCR–pMHC complexes (10, 11), there have been no TCR–pMHC structures determined that address the effect on TCR recognition of only anchor residue modifications. However, an example of the impact of changes at buried MHC class I residues on TCR recognition has been provided by Luz and colleagues (12).

Several studies have sought to relate the structural characteristics of the TCR–pMHC interface with TCR binding affinities (13, 14). TCR binding is characterized by low affinities (0.1–57 μM) and a degree of cross-reactive recognition (15, 16). Although peptide analogs bearing substitutions at anchor residues have been used in several clinical trials (1), neither the structural effect of these changes, nor how such features correlate with enhanced immunogenicity in vivo are well understood. It is important to analyze the molecular basis for the improved immunological potency of peptide analogs, because such information may provide guidelines for the rational design of T cell vaccines. Ideally, the properties of superagonist peptide analogs would blend (a) high affinity and stability of binding to the MHC class I molecule, (b) TCR binding properties that elicit potent and effective T cell expansions, and (c) high levels of TCR cross-reactivity to the endogenous target epitope on vaccination in vivo.

NY–ESO-1 is one of the most promising tumor-specific antigens, which was identified by the application of serological analysis of recombinant cDNA libraries from human tumors (17, 18). NY–ESO-1 is expressed by a broad range of tumor types (17). Vaccines designed to boost CTL responses against NY–ESO-1 epitopes may therefore be useful in the treatment of many tumors. The A2-restricted NY–ESO-1 T cell response has been identified using NY–ESO-1–specific CTL lines derived from melanoma patients and shown to be specific for the epitope NY–ESO-$1_{157–165}$ (18). To investigate the structural and kinetic features of TCR recognition of A2 loaded with the wild-type NY–ESO-$1_{157–165}$ peptide (SLLMWITQC; hereafter referred to as "ESO 9C peptide") we produced a soluble version of a NY–ESO-$1_{157–165}$–spe-

Table I. Crystallographic statistics

	1G4–A2–9C	1G4–A2–9V	1G4
Data collection			
Space group	$P2_1$	$P2_1$	$P2_1$
Unit cell			
Dimensions (Å) (a, b, c)	73, 63, 117	73, 63, 117	43, 60, 83
Angles (°) (α, β, γ)	90, 105, 90	90, 107, 90	90, 90, 90
Source (λ Å)	ESRF ID14eh2	ESRF ID14eh2	ESRF ID14eh2
Resolution (Å) (highest resolution shell)	20 − 1.9 (1.97 − 1.90)[d]	20 − 1.7 (1.76 − 1.7)[d]	20 − 1.4 (1.46 − 1.4)[d]
Measured reflections	994978	948573	696843
Unique reflections	87826	112638	85029
Completeness (%)	98.5 (96.6)[d]	89.3 (49.5)[d]	93.0 (62.7)[d]
I/σ (I)	9.8 (1.5)[d]	19.4 (2.0)[d]	24.7 (4.3)[d]
R_{merge} (%)[a]	6.0 (45)[d]	7.8 (58)[d]	7.8 (32)[d]
Refinement statistics			
Resolution range (Å)	20 − 1.9 (1.97 − 1.90)[d]	20 − 1.7 (1.76 − 1.7)[d]	20 − 1.4 (1.46 − 1.4)[d]
R_{cryst}[b]	23.0	22.6	24.5
R_{free}[c]	26.0	25.3	26.5
Number of residues	829	829	444
Number of water molecules	505	512	243
Rms deviation from ideality			
Bond lengths (Å)	0.006	0.05	0.005
Bond angles (°)	1.7	1.3	1.3
Percent Ramachandran plot (favored, allowed, generous, disallowed)	(90.5, 9.0, 0.4, 0.0)	(89.6, 10.1, 0.3, 0.0)	(85.6, 13.1, 1.3, 0.0)

[a] $R_{merge} = \Sigma_{hkl}|I - <I>|/\Sigma_{hkl}I$ where I is the intensity of unique reflection hkl and <I> is the average over symmetry-related observation of unique reflection hkl.
[b] $R_{cryst} = \Sigma|F_{obs} - F_{calc}|/\Sigma F_{obs}$ where F_{obs} and F_{calc} are the observed and calculated structure factors, respectively.
[c] R_{free} is calculated as for R_{cryst} but using 4.4% of reflections sequestered before refinement.
[d] Numbers in parentheses correspond to the outermost shell of data.

cific TCR. Our initial analysis revealed that TCR interactions with this native epitope are dominated by two highly exposed residues, methionine and tryptophan, whose side chains protrude from the central part of the peptide (at positions 4 and 5). The presence of this prominent hydrophobic feature suggests that for this system TCR binding in general will focus on the central region of the peptide and be relatively tolerant of changes in the pMHC surface near the peptide carboxyl terminus. To test this hypothesis and its implications for the immunogenic characteristics of the system, we performed a series of studies to provide structural, solution binding, in vitro functional and in vivo immunogenic data. Because we had previously demonstrated that substitution of the cysteine to valine at position 165 (19) enhances the ability of the epitope to be recognized in vitro by NY–ESO-$1_{157–165}$–specific CTL, we focused on this peptide analogue (SLLMWITQV; hereafter referred to as "ESO 9V peptide"). Our results provide insights into the mechanisms controlling the enhanced immunogenicity of superagonist peptides by demonstrating a correlation between the stability of the peptide–MHC–TCR complex, its ability to stimulate a faster formation of conjugates, resulting in polarization of lytic granules, killing of target cells, and in vivo proliferation.

RESULTS

Structure of the TCR and ESO 9C–A2 complex

Structural studies were performed using soluble, purified TCR (6) from the NY–ESO-$1_{157–165}$–specific 1G4 CTL clone (hereafter 1G4 TCR). The 1G4 TCR–A2–ESO 9C complex crystal diffracted to 1.9 Å resolution and contained one complex per asymmetric unit (Table I). A 1.4-Å resolution crystal structure was also determined for the unliganded 1G4 TCR. In the complex structure the orthogonal binding orientation of the 1G4 TCR with respect to the long axis of the ESO 9C peptide (69°) lies at one extreme of the range observed, to date, for TCR–pMHC class I interactions and is very similar to the orientation observed for the JM22 TCR–A2–influenza matrix peptide complex (20). These two structures, plus that recently reported for the TCR AHIII–A2–p1049 complex (21), establish that there is significant overlap between the binding orientations for class II– and class I–restricted TCR recognition.

The 1G4–A2–ESO 9C complex displays a prominent methionine–tryptophan (MW) "peg" in the central P4/P5 portion of the peptide, which forms a large protrusion from the surface of the pMHC (Fig. 1, A and B). The 1G4 TCR envelops this protrusion between its complementarity determining region (CDR) loops, making contacts via the CDR3α,CDR3β and CDR1α loop residues. In previous pMHC–TCR complex structures, a single upward pointing residue from the peptide has often formed a peg about which the TCR CDR loop residues cluster making contacts conferring specificity and affinity (5, 22, 23). In this case, the peg is composed of a double side chain motif. This bulky and hydrophobic structure provides the majority of interactions between the epitope and the 1G4 TCR. More generally, given its central position within the TCR recognition surface, it seems probable that the MW peg constitutes the dominant antigenic feature of this peptide (Fig. 1 A).

The total solvent-accessible surface area buried at the 1G4 TCR–A2–ESO 9C interface is ~1,440 Å^2 with the TCR contribution being split relatively equally between α and β chains, 46% and 54%, respectively. Of this total 730 Å^2 (~50%) results from TCR–peptide interactions with 49% of the buried surface area between the ESO 9C peptide and the 1G4 TCR accounted for solely by interactions involving the MW side chains (360 Å^2). Analyses of the shape complementarity at the interface between the 1G4 TCR and (a) the pMHC (S_c = 0.71), (b) the entire ESO 9C peptide (S_c = 0.83), and (c) specifically the MW side chains (S_c = 0.87) demonstrate that there is a very high degree of shape complementarity to the epitope, in particular to the MW peg. Rudolph and colleagues calculated S_c values ranging from 0.41 to 0.66 (with most clustered between 0.61–0.66) for the nine TCR–pMHC complex structures available in 2002 (5). Where the resolution of the x-ray diffraction data is sufficient for conserved water molecules to be included in the structure, these are frequently found to be integral to the pMHC–TCR interactions (12, 20, 24). For example, in the JM22–flu matrix$_{58–66}$–HLA–A2 complex S_c equals 0.73, with interfacial waters included in the calculation, and 0.64 without (20). The 1G4 TCR–A2–ESO 9C interface is notable in that it achieves high S_c values without any contribution from interfacial water, because the interface between the MW side chains and the TCR CDR3αCDR3β and CDR1α loops contains no trapped water molecules. The core of the 1G4 TCR–A2–ESO 9C interface is stabilized by hydrophobic and ring-stacking interactions, consistent with the hydrophobic and aromatic nature of the peptide M and W side chains (Fig. 1, C and D). Instead, water molecules cluster at the periphery of this pMHC–TCR interface, forming a belt associated with the peptide, TCR and A2, which may contribute to the thermodynamic properties of 1G4 TCR recognition (unpublished data).

Previous studies that have compared TCR structures in unbound and complexed states (25–29) report remarkably large (up to 15 Å) conformational changes in the CDR3 α and β loops. Although the 1G4 TCR uses a substantial cavity to accommodate the MW peg between its CDR1α, CDR3α, and CDR3β loops (Fig. 1 C), this cavity is preformed (Fig. 1 E). In contrast with the mechanisms of induced TCR fit reported for other pMHC–TCR complexes, a well optimized binding surface is achieved by relatively small structural changes. Comparison of the unliganded and liganded 1G4 TCR structures reveals only relatively minor main chain shifts in all the CDRβ loops (for example, <1.6 Å for V96β at the tip of the CDR3β; Fig. 1, C and E). The largest main chain shifts (up to 4.2 Å) in the Vα domain also occur at the tip of the CDR3 loop resulting from a change in the main chain conformation of residues 95–99. Only

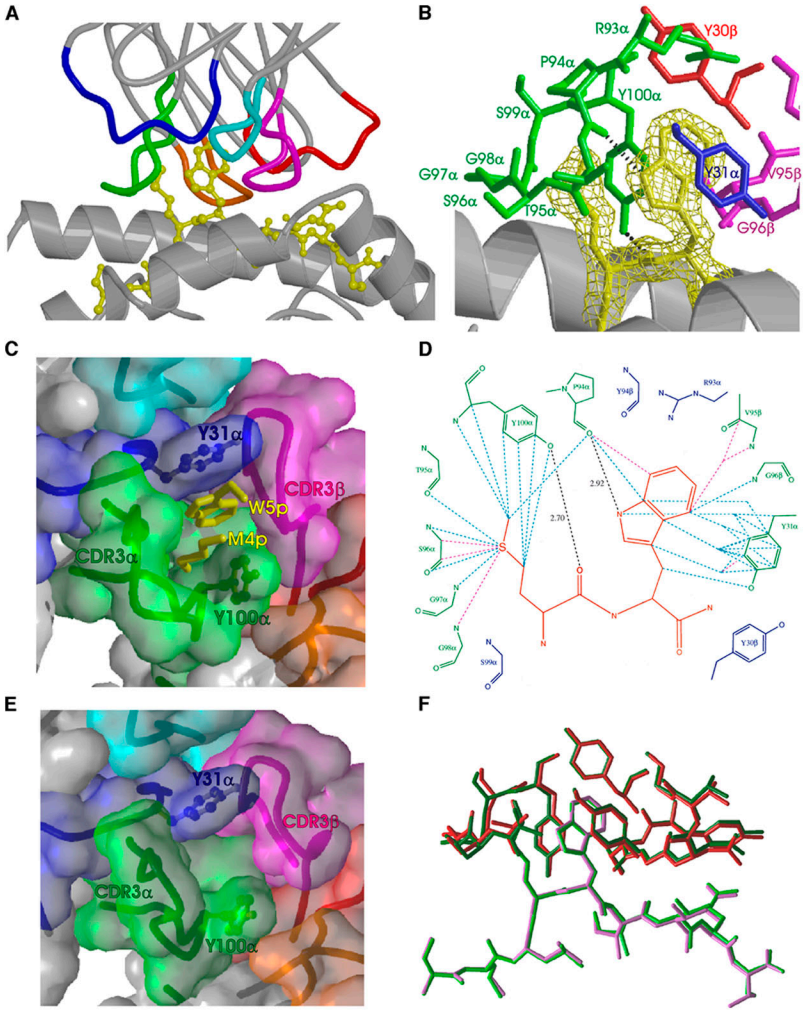

Figure 1. Structure of 1G4 TCR bound to A2–NY–ESO–1 complexes. (A) Diagram highlighting the CDR loops of the 1G4 TCR complexed to the A2–ESO 9C. The CDR loops are colored as follows: V_αCDR1, blue; V_αCDR2, cyan; V_αCDR3, green; V_βCDR1, red; V_βCDR2, orange; and V_βCDR3, magenta. The peptide (yellow) projects a bulky methionine-tryptophan peg, which is embedded deep within the TCR CDR loops. (B) Simulated annealing omit electron density map yellow chicken wire showing the M_4W_5 residues bound by the 1G4 TCR. TCR contact residues are colored according to CDR color as in panel A. Hydrogen bonds between the $CDR3_\beta$ and the M_4W_5 residues are shown in black. The map is contoured at 3σ. (C) Illustration of the complexed TCR colored according to panel A, and showing the close interaction of the hydrophobic peptide MW peg (yellow) with the TCR Y31α and Y100α side chains. (D) Schematic diagram showing the interactions between the M_4W_5 peg residues and the surrounding 1G4 TCR residues. TCR contact residues with a minimum interatomic distance of ≤3.8 Å are shown in green, whereas other residues surrounding the M_4W_5 peg are shown in blue. The individual distances between the TCR and the M_4W_5 peg are shown as dashed lines (distances ≤3.4 Å are shown in pink; distances between 3.4 Å and 3.8 Å are in light blue; hydrogen bonds are shown with distances in black). (E) View of the TCR antigen combining surface from the perspective of pMHC with CDR loop surfaces colored according to panel A. The figure shows the structure of the uncomplexed TCR, highlighting the $Y30_\alpha$ and $Y100_\alpha$ side chains. (F) α1α2 helix superimposition of the ESO 9C (green peptide and dark-green TCR) and ESO 9V (pink peptide and red TCR) TCR–peptide structures showing the subtle differences the anchor residue modification propagates throughout the complex interface. Notably, the COOH-terminal half of the ESO 9C peptide is 0.6 Å further out of the HLA-A2 groove than the 9V peptide and the tip of the $CDR3_\beta$ loop is lower compared with the TCR–A2–ESO 9V complex.

subtle adjustments in preexisting (unliganded) side chain conformations appear to be required to optimize the interaction of Y100α with the peptide at M4 and ring-stacking interactions between Y31α and the W5 side chain. However, these TCR residues show a considerable reduction in flexibility on engagement with the MW peg (average crystallographic temperature factors for the side chain atoms of Y31α are 36 $Å^2$ unliganded and 23 $Å^2$ liganded, and for Y100α the values are 50 $Å^2$ unliganded and 22 $Å^2$ liganded).

Comparison of the 1G4 TCR–ESO 9C–A2 and 1G4 TCR–ESO 9V–A2 complexes

Because the 1G4 TCR recognition appears to be so focused on the central region of the peptide, we wished to assess

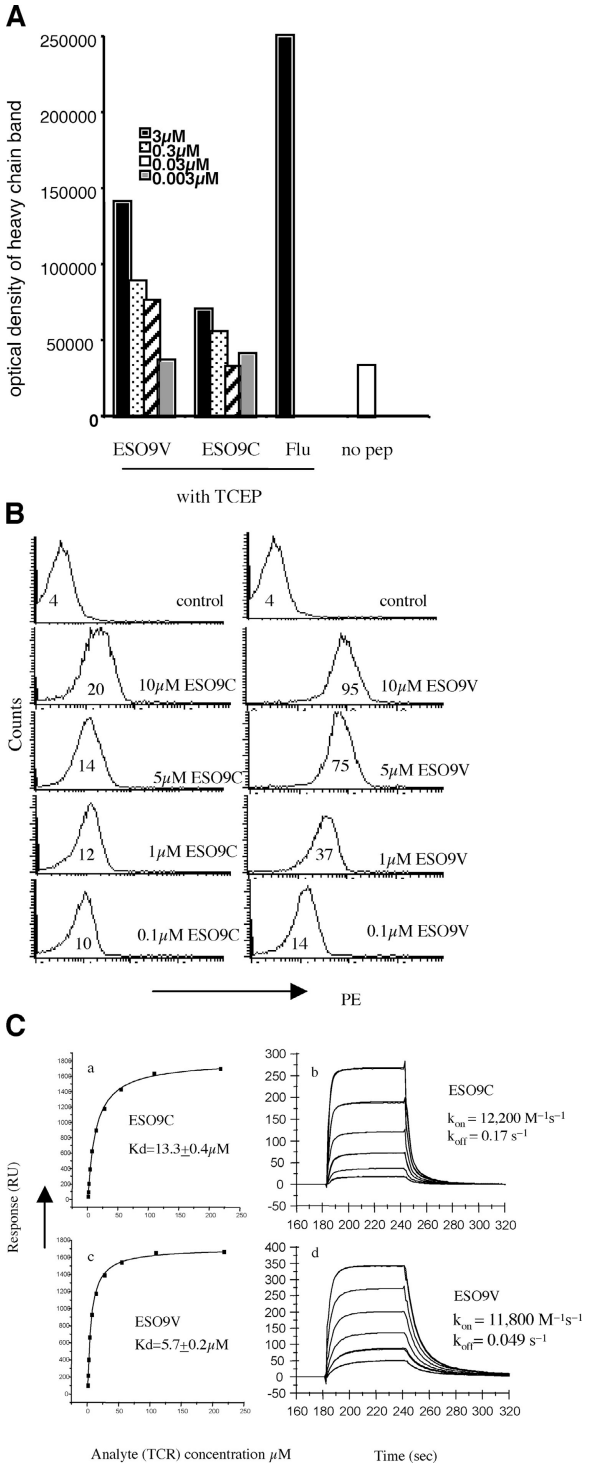

Figure 2. Binding measurements of peptide to A2 molecules and pMHC complex to TCR. (A) HLA A2–peptide complexes were precipitated from T2 lysate pulsed either with ESO 9C or ESO 9V peptide at concentrations shown. HLA-A2 molecules from T2 cells pulsed with either 3 μM flu matrix58–66 peptide or in the absence of peptide (open bar) were used as positive and negative controls. ESO 9C, ESO 9V, and flu matrix58–66 peptides were treated with 20 mM TCEP at room temperature for 1 h before being added to the T2 cell lysate at the final concentration of 200 μM. (B) T2 cells were stained with the A2–ESO 9C-specific Fab antibody 3M4E5. T2 cells were pulsed with either ESO 9C (left column) or ESO 9V (right column) at concentrations shown. Negative control staining with flu matrix peptide is shown in the top panel. Mean channel fluorescence is shown in each panel. (C) Affinity measurements for TCR binding to A2 complexed with ESO 9C and ESO 9V are shown in panels a and b and c and d, respectively. Panels a and c show measurements at equilibrium, whereas panels b and d show kinetic measurements. Panels a and c show 10 serial dilutions in duplicates of 1G4 NY–ESO-1–TCR (analyte), starting from a concentration of 240 μM. Panels b and d show six serial dilutions in duplicates of 1G4 NY–ESO-1–TCR, starting from a concentration of 24 μM.

whether substitutions of the carboxyl-terminal residue of the NY–ESO-1 peptide could alter the peptide structure and affinity of interaction with the 1G4 TCR. Because we have previously shown that substitution of cysteine to valine at position 165 of the NY–ESO-$1_{157–165}$ epitope enhanced its ability to sensitize target cells for killing by the 1G4 CTL clone (19), we decided to focus further structural studies on the 9V NY–ESO-1 peptide analogue (ESO 9V).

The crystal structure of the 1G4 TCR–A2–ESO 9V complex was determined at 1.7 Å resolution from crystals of the same space group and essentially identical unit cell dimensions to those used for the 1G4–A2–ESO 9C structure. To a first approximation the two complex structures are very similar. Structural comparison reveals that substitution of the cysteine to valine causes little difference in the general orientation of the side chain within the F pocket of the A2 peptide binding groove. Changes in the positions of the A2 side chains constituting the F pocket are also minimal. However, the relatively high resolution of both the 1G4–A2–ESO 9C and 1G4–A2–ESO 9V crystal structures permits a detailed analysis (Fig. 1 F). It is evident that the ESO 9V side chain is buried deeper into the F-pocket and occupies a slightly larger volume than the cysteine side chain. Both the shape complementarity and the buried surface within the F-pocket is greater for ESO 9V compared with ESO 9C (side chain surface areas: ESO 9V = 191 Å^2, ESO 9C = 162 Å^2 and shape complementarities: ESO 9V = 0.81, ESO 9C= 0.72). These changes are sufficient to enhance significantly the van der Waal's contacts between the altered peptide ligand and A2, in line with this MHC class I molecule's reported preference for valine as COOH-terminal anchor residue (30).

The changes in the position of the COOH-terminal anchor residue, resulting from the C9V substitution, propagate through the peptide main chain resulting in the P6–P8 region being positioned slightly deeper (0.3 Å) within the A2 peptide binding groove. Although the P6–P8 region of the peptide has fewer contacts with the 1G4 TCR than the MW peg at P4 and P5, the structural difference in the peptide is clearly transmitted to the TCR (Fig. 1 F). The angle of engagement made by the 1G4 TCR differs between the peptide complexes by some 0.9°. This is essentially a change in the TCR's tilt, relative to an axis drawn perpendicular to the pMHC binding surface, in response to the lower position of the main chain COOH-terminal half of the ESO 9V peptide. Numerous small changes are discernible at the complex

interface. These changes are focused on residue Q155 of the A2 α2 helix. For the A2–ESO 9V complex the Q155 side chain is well ordered and makes hydrogen bonds to the Oγ atoms of S52 and S53 side chains. In contrast, for the A2–ESO 9C complex the Q155 side chain is relatively disordered and appears to be sampling an additional conformation, forming a hydrogen bond to T95α on the CDR3α loop of the 1G4 TCR. The change in TCR tilt of the A2–ESO 9V complex precludes the latter option and the CDR3α loop adopts a less well ordered structure. The average B-factor for residues in the tip of CDR3α loop (all atoms in Ser96 α and Gly97 α) are 33.93 and 42.46 for the A2–ESO 9C and A2–ESO 9V complexes, respectively. Analysis of the shape complementarity between the 1G4 TCR and the pMHCs suggests a slightly better overall fit is achieved with A2 /ESO 9V ($S_c = 0.73$) compared with A2–ESO 9C ($S_c = 0.71$). The significance of this difference in S_c is discussed in Materials and methods. The difference includes tighter interactions between TCR and variant peptide (ESO 9V peptide $S_c = 0.85$; ESO 9C peptide $S_c = 0.83$).

Enhanced binding affinity of ESO 9V peptide for A2 molecules and slower 1G4 TCR dissociation rate from the ESO 9V–A2 complex

Our comparison of the ESO 9C- and ESO 9V-based complex structures revealed the substitution of cysteine at position 9 by valine provides an improved fit to the A2 F pocket, a result that might be expected on the basis of established anchor preferences. However, this substitution, at a position buried within the binding groove, was also revealed to trigger subtle, but significant, changes at the TCR–pMHC interface. To correlate these structural features of the TCR–pMHC complexes with kinetics of binding, we assessed the affinity of binding of the ESO 9V and ESO 9C peptides to A2 molecules, and the affinity of 1G4 TCR binding to A2 molecules loaded with either the ESO 9V peptide or the wild-type ESO 9C peptide. Binding of ESO 9V peptide to A2 molecules was compared with that of ESO 9C by measuring peptide binding to metabolically labeled A2 molecules in T2 cells (31). Measurement of the optical density of metabolically labeled A2 SDS gel bands showed that ESO 9V peptide can stabilize a higher proportion of A2 molecules than the ESO 9C peptide (Fig. 2 A).

To confirm these results, experiments were performed using the 3M4E5 Fab antibody specific to NY–ESO-$1_{157–165}$–A2 complexes (32). Initial Biacore measurements demonstrated that the 3M4E5 Fab antibody recognizes A2 molecules loaded with either ESO 9V or ESO 9C peptide with a similar affinity of ~60 nM (unpublished data). FACS staining with the 3M4E5 antibody of T2 cells pulsed with different concentrations of ESO 9V and ESO 9C peptides confirmed that ESO 9V peptide binds to A2 molecules with greater efficiency than the ESO 9C peptide (Fig. 2 B).

Surface plasmon resonance affinity measurements were performed using the soluble form of 1G4 TCR in order to compare the affinity of binding of a NY–ESO-$1_{157–165}$–specific TCR to A2 molecules loaded with either the wild-type ESO 9C peptide or the ESO 9V analogue. The experiments demonstrated a higher affinity of binding for the 1G4 TCR to the A2–ESO 9V complex than to the A2–ESO 9C complex (Fig. 2 C). Analysis of the binding curves of conformation-specific anti-A2–peptide and anti-β2M antibodies con-

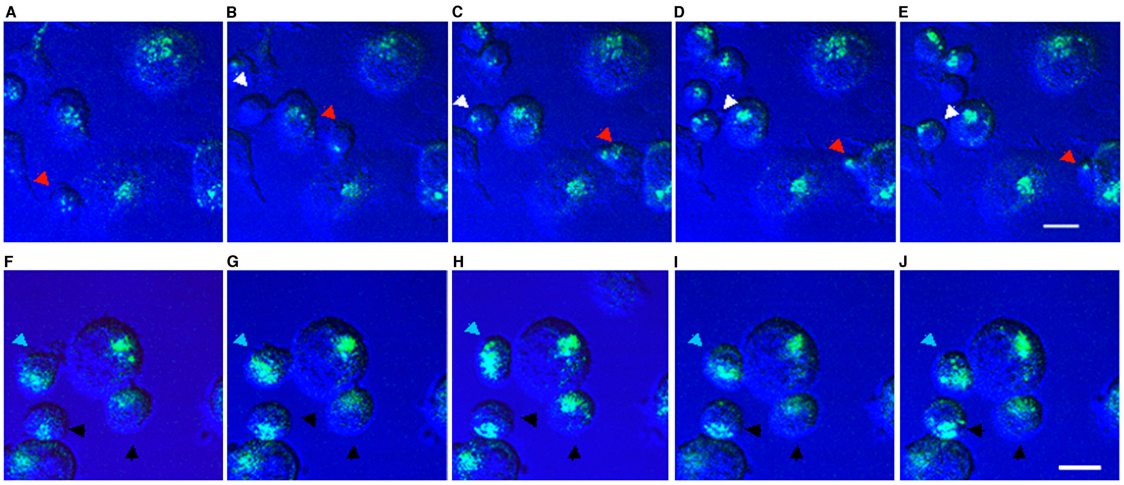

Figure 3. 1G4 CTL–T2 conjugates formation is very efficient when targets are loaded with ESO 9V peptide. The panel shows a series of selected images taken from the live-cell videos in Videos 1 and 2 (available at http://www.jem.org/cgi/content/full/jem.20042323/DC1). CTLs loaded with lysotracker green were added to the adherent T2 target cells pulsed with 1 μM ESO 9C (A–E; and Video 1) or pulsed with 1 μM ESO 9V (F–L; and Video 2). The images selected from the Video 1 correspond to time 0 (A) indicating the first contact of a CTL with T2 pulsed with ESO 9C, 5 min (B), 12 min, and 20 s (C), 15 min and 20 s (D), 22 min and 40 s (E) and the ones taken from Video 2 are, respectively: time 0 (F), 1 min and 40 s (G), 5 min and 40 s (H), 6 min and 20 s (I), and 9 min and 40 s (L). The Normaski differential interference contrast image (blue) and 1 μM of green confocal image have been super-imposed at each time point. White, red, black, and light blue arrows indicate the CTLs described in the results. Bars, 10 μm.

firmed that equivalent amounts of correctly refolded A2–peptide complexes were immobilized to the Biacore chips (Fig. S1, A and B). Good agreement was observed between the affinities determined kinetically (the ratio of K_{off} to K_{on}) and those determined by equilibrium measurements. The equilibrium binding constants (K_d) at 25°C for the soluble 1G4 TCR binding to A2 loaded with the ESO 9V or ESO 9C peptide were determined to be 5 and 13.3 μM, respectively (Fig. 2 C). Kinetic measurements demonstrated that the higher affinity of binding was predominantly due to a slower off rate for the 1G4 TCR when bound to the A2–ESO 9V complex compared with the A2–ESO 9C complex. The slower off-rate is in line with the structural data, which indicate that more pMHC–TCR contacts form at the ESO 9V interface than at the ESO 9C interface.

ESO 9V induces polarization of CTL granules more efficiently than the wild type

To assess the functional consequences of the differences in pMHC and TCR–pMHC binding affinities, we analyzed the rate of polarization of cytotoxic T cell granules on stimulation of a NY–ESO-$1_{157–165}$–specific CTL clone with target cells pulsed with either the ESO 9C or the ESO 9V peptides. These experiments were performed with the same 1G4 CTL clone for which the structural and kinetic studies had been derived.

When T2 cells are pulsed with 1 μM ESO 9C peptide (Video S1 and Fig. 3, A–E), lytic granule polarization is slow. Fig. 3, A–E, shows two CTLs from contact to polarization. In one case (white arrow) granule polarization from the periphery (Fig. 3 B) to the synapse (Fig. 3 E) occurs within 17 min after the initial contact. In the other example (red arrow), the CTL first crawls under one target (Fig. 3, A and B) before contacting a new target (Fig. 3 C) without polarization of the lytic granules toward either target in >22 min. In contrast, granule polarization is rapid when T2 targets are pulsed with 1 μM ESO 9V peptide (Video 2 and Fig. 3, F–L). For one CTL, from the first encounter (Fig. 3 F, green arrowhead) to granule polarization (Fig. 3 L) the elapsed time is 4 min. Other CTLs in the field being filmed (Fig. 3 L, black arrowheads) had already polarized their granules toward targets by the time images were captured.

CTL and target cells were mixed with different concentrations of the two peptides, incubated at 37°C for 30 min and fixed in order to provide quantitative data with a large number of conjugates. Lytic granules were labeled with antibodies against cathepsin D (Fig. 4 A, a–c, green) and the p58 Golgi protein (Fig. 4 A, a–c, red). Both the Golgi apparatus and granules polarize upon CTL recognition of target (33), and the degree of polarization in CTL conjugated to targets were counted according to whether granules and Golgi proteins were located (a) at the rear of the CTL (Fig. 4 A, a, un-

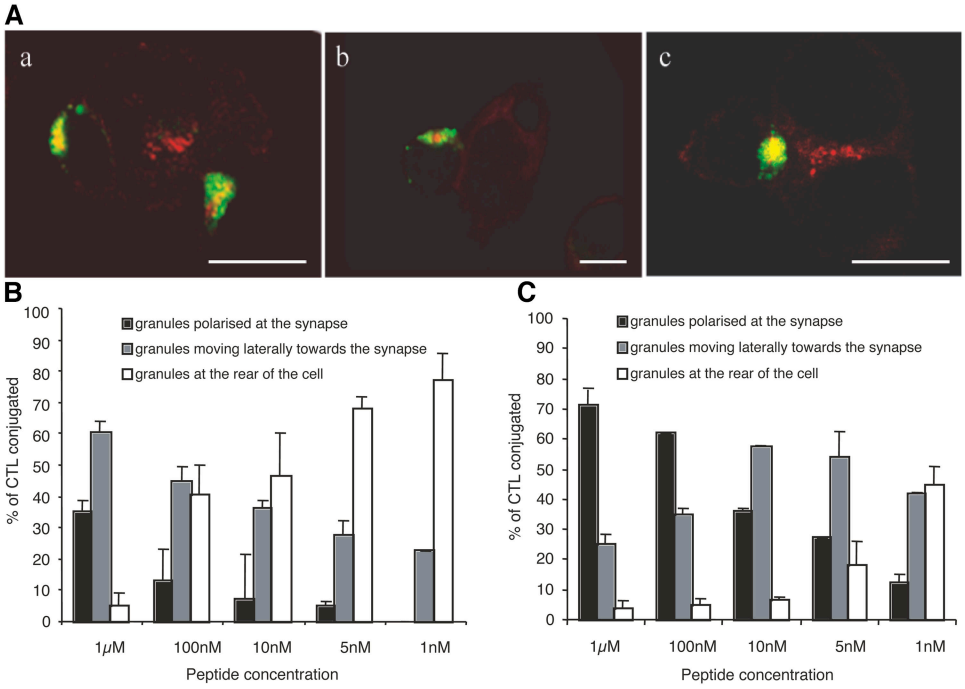

Figure 4. ESO 9V is very efficient in inducing polarization of CTL granules at the immunological synapse. (A) The confocal images show 1G4 CTLs conjugated with T2 pulsed with 1 μM ESO 9V. Lytic granules stained with anti-cathepsin D (green) and anti-p58 cis Golgi protein (red). Upon target cell recognition both Golgi and lytic granules move from the rear of the cell (a), around the nucleus (b), and polarize at the immunological synapse (c). (B and C) Quantitative analysis of granule polarization in 1G4 CTL clone recognizing targets pulsed with ESO 9C (B) or ESO 9V peptides (C). Cell conjugates with granules at the rear (white bar), granules moving laterally toward the synapse (gray bar) and granules at the synapse (black bar) as illustrated in A were counted using a fluorescence microscope.

polarized); (b) at the side of the CTL (Fig. 4 A, b, polarizing); or (c) polarized at the immunological synapse (Fig. 4 A c). When T2 cells were pulsed with the ESO 9C peptide polarization was poor (Fig. 4 B) and 1 μM of peptide was required to see 30% of conjugates with tightly polarized granules at the synapse. By comparison, for ESO 9V granule polarization is much more efficient and only 0.01 μM ESO 9V peptide is required to see 30% of polarized CTL (Fig. 4 C). The higher percentage of target cell killing (19) and secretion of lymphokines (Fig. 5) may therefore reflect the shorter times required for CTL to recognize and destroy individual targets.

Differential role of CD8 binding in CTL recognition of A2–ESO 9V and A2–ESO 9C

We sought to assess whether the CD8 requirement of the 1G4 NY–ESO-$1_{157–165}$–specific CTL clone differed for the recognition of wild-type ESO 9C or ESO 9V analogue peptides (Fig. 5). We show that recognition of the ESO 9V peptide is less CD8 dependent than recognition of the ESO 9C peptide, because CTL recognition of ESO 9C was significantly more efficient in the presence of A2 molecules bearing a CD8 binding site. These results also confirm that the 1G4 CTL clone is up to 100 times more sensitive to the ESO 9V peptide compared with the ESO 9C peptide.

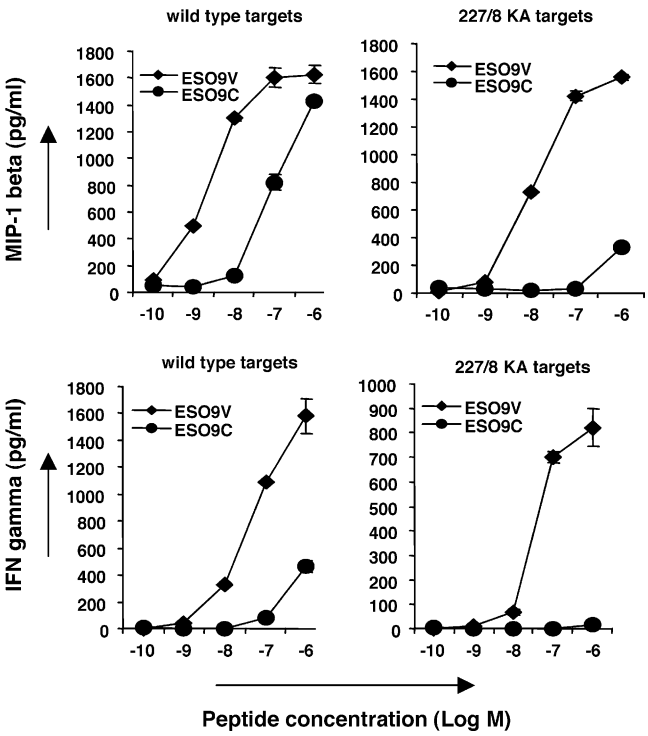

Figure 5. Role of CD8 in the recognition of the ESO 9V and ESO 9C peptides. CIR B cells transfected with either wild-type A2 or A2 DT227/8KA were pulsed with either ESO 9V or ESO 9C peptides. Supernatant was assayed for MIP-1β (top) or IFN-γ (bottom) by ELISA. Standard deviation from the mean of two duplicate assays is shown. Diamonds indicate target cells pulsed with ESO 9V peptide. Circles indicate target cells pulsed with ESO 9C peptide.

Enhanced in vivo immunogenicity of ESO 9V peptide analogs

We assessed whether the ESO 9V peptide is capable of expanding in A2 transgenic mice greater numbers of NY–ESO-$1_{157–165}$–specific CTL that are cross reactive to the native epitope. The results show that recombinant vaccines encoding the ESO 9V peptide are capable of inducing stronger NY–ESO-$1_{157–165}$ responses than vaccines encoding the wild-type ESO 9C peptide, both in terms of percentages of responding mice and frequency of the T cell response induced (Fig. 6 A). Furthermore, ESO 9V–primed mice were capable of recognizing the wild-type ESO 9C peptide, as defined by ex vivo tetramer staining with $A2K^b$ tetramers loaded with the ESO 9C peptide (Fig. 6 B). The proportion of NY–ESO-$1_{157–165}$–specific CTL, stained by $A2K^b$ tetramers loaded with either the ESO 9C or the ESO 9V peptide was very similar. Consistent with these findings, in vitro killing assays showed that NY–ESO-$1_{157–165}$–specific CTL, generated from ESO 9V–immunized mice, were capable of lysing target cells loaded with wild-type ESO 9C peptide, as well as target cells loaded with the ESO 9V analogue (Fig. 6 C). IFN-γ ELISPOT assay was used to assess further cross reactivity and the function of these CTL. CTL generated from animals immunized with the ESO 9V sequence were capable of producing IFN-γ in response to ESO 9C peptide. As expected, responses were enhanced in the presence of the reducing agent TCEP, which prevents cysteinylation and dimerization of ESO 9C peptide (unpublished data (19, 34). Finally, a larger proportion of ESO 9V–primed T cells was capable of secreting IFN-γ, when stimulated by target cells pulsed with ESO 9C peptide, than ESO 9C primed T cells (Fig. 6 D). Enhanced IFN-γ response by T cells from ESO 9V–primed mice was not due to the higher numbers of ESO 9V–primed T cells, because the numbers of splenocytes from ESO 9V and ESO 9C primed mice added to the ELISPOT plates were normalized for the percentage of ESO 9C tetramer positive T cells.

DISCUSSION

Previous studies (35) have raised the issue that changes in peptide anchor residues can directly affect TCR recognition, as well as pMHC stability. Such effects have important implications for T cell cancer vaccines. A2–ESO 9C represents a clinically relevant system in which we can assess the factors that will need to be considered when engineering vaccine epitopes. Because it is known that cysteinylation may reduce antigenicity of synthetic peptides binding to MHC class I molecules (34), we sought to study whether modification of cysteine 165 in the NY–ESO-$1_{157-165}$ epitope would increase its immunogenicity. Our results demonstrate that modification of cysteine to valine at position 165 of NY–ESO-$1_{157–165}$ both augments epitope binding to MHC and heightens TCR affinity. These two properties act in concert to gener-

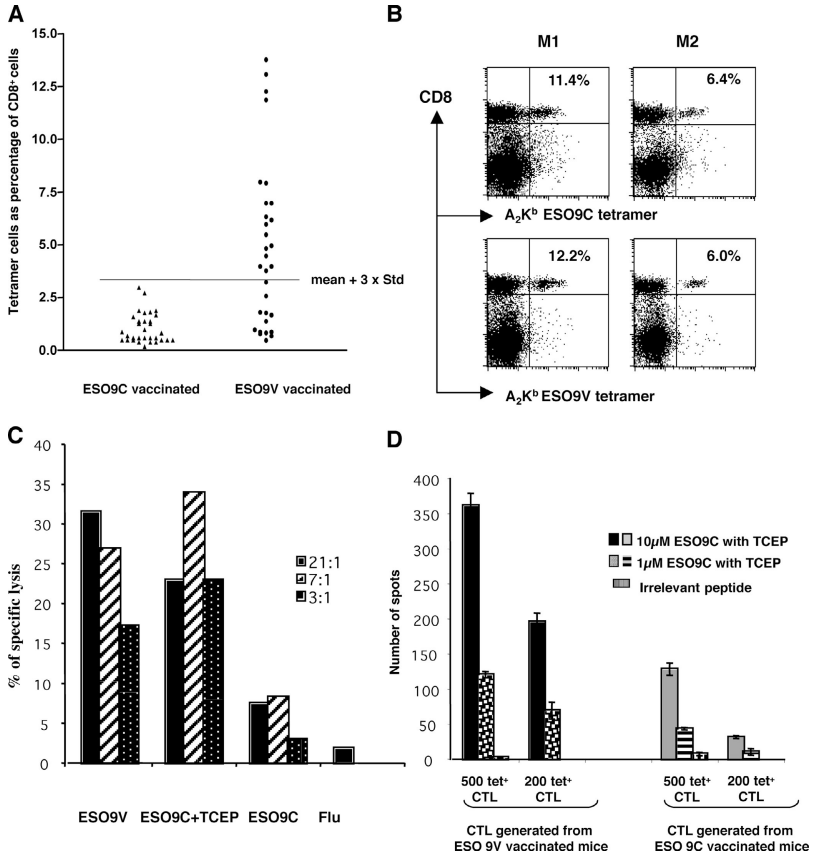

Figure 6. Enhanced in vivo immunogenicity of ESO 9V vaccines. (A) A2K^b transgenic mice were immunized with plasmid DNA followed by recombinant vaccinia virus encoding either ESO 9C or ESO 9V peptides. Splenocytes from immunized mice were stained ex vivo 1 wk after vaccinia injection with A2K^b tetramers loaded with ESO 9C peptide (57). Results from four separate experiments were combined, each experiment includes five to eight mice ($P = 0.0001$). (B and C) Splenocytes from ESO 9V–immunized mice are capable of recognizing ESO 9C peptide. B shows that PBL from mice immunized with ESO 9V vaccines were ex vivo stained with A2K^b tetramers containing either ESO 9C (top row) or ESO 9V (bottom row) peptides. Percentage of tetramer$^+$ of CD8$^+$ cells is shown in each panel. C shows lysis of target cells (Jurkat cells transfected with A2K^b cDNA) pulsed with either ESO 9V or ESO 9C peptide. Target cells pulsed with the irrelevant peptide flu matrix58–66 (Flu) were used as negative controls. To ensure optimal presentation of the ESO 9C peptide, lysis of target cells pulsed with ESO 9C peptide was compared in the presence or absence of the reducing agent TCEP. In agreement with our previous results (19), ESO 9C pulsed target cells were killed more efficiently in the presence of the reducing agent TCEP (ESO 9C+TCEP) than in the absence of TCEP (ESO 9C). (D) Enhanced IFN-γ response by T cells from ESO 9V–primed mice. Splenocytes from either ESO 9V– or ESO 9C–immunized mice were tested for their ability to recognize target cells pulsed with ESO 9C peptide. Duplicate samples were used. Peptide concentrations and numbers of tetramer positive T cells are shown.

ate stronger T cell cytolysis and activation, without compromising cross-reactivity with the wild-type peptide. Valine, while optimizing the anchoring of the peptide in the A2 F pocket, does not alter the orientation and height of the peptide's prominent methionine–tryptophan TCR binding motif. However, subtle repositioning of the peptide main chain introduces some small but significant changes at the pMHC–TCR interface which appear sufficient to generate a lower TCR K_{off} rate.

To elicit effective antitumor responses, it is important to develop strategies capable of reversing T cell tolerance to tumor antigens and jump starting the immune response to expand rapidly greater numbers of tumor-specific CTL. Although previous papers have correlated higher affinity of peptide binding to MHC class I molecules and TCR with increased immunogenicity (36–40), none of the previous studies have compared functional data to structural and kinetic analyses.

The use of a Fab antibody specific to the A2/NY–ESO-$1_{157–165}$ peptide complex (32) permits comparison of the efficiency of ESO 9C and ESO 9V binding to surface expressed A2 molecules (Fig. 2 B). The results of these experiments are consistent with ~100-fold difference in binding affinity to A2 molecules between the ESO 9C and ESO 9V peptides. They also show that, within the range of peptide concentrations used for the analysis of granule polarization (Figs. 3 and 4) and cytokine secretion (Fig. 5), cells pulsed with ESO 9V peptide present to the 1G4 CTL clone approximately three- to five-fold more peptide than cells pulsed with the ESO 9C peptide. These results suggest that the enhanced effector functions of

the 1G4 CTL clone stimulated by ESO 9V peptide can be accounted for by a combined effect of higher peptide affinity to A2 molecules and slower off rate of the 1G4 TCR from the ESO 9V–A2 complex. These results are consistent with previously published data demonstrating enhanced antigen-specific antitumor immunity with altered peptide ligands (40), although for the system studied by Slansky and colleagues the effect is entirely due to a threefold slower pMHC–TCR off rate. Although lytic granule polarization formed in response to maximal pMHC densities has been extensively characterized, fewer reports have examined variations in the efficiency of lytic granule polarization with peptide density (41). The results of our confocal microscopy experiments (Fig. 4) highlight variations in the efficiency of lytic granule polarization over a range of different peptide concentrations and different stability of TCR–pMHC complexes.

Increased immunogenicity in A2 transgenic mice and enhanced expansion of NY–ESO-1–specific CTL from melanoma patients' PBL demonstrate that the enhanced stimulation of the clone 1G4 can be extended to a polyclonal population. Although we cannot rule out the possibility that in vivo results can mainly be accounted for by the higher affinity of binding of the ESO 9V peptide to A2 molecules, it is of interest that NY–ESO-$1_{157–165}$–specific T cells from ESO 9V–primed mice have an enhanced ability to recognize target cells pulsed with the ESO 9C peptides, as compared with NY–ESO-$1_{157–165}$–specific T cells from ESO 9C primed mice (Fig. 6 D). It is possible that this enhanced T cell activity could be due to the increased stability of the ESO 9V–A2 complex resulting in differences at the level of the immunological synapse at the T cell–DC interface and in the expansion of better quality T cells. Consistent with this possibility, differences in the molecular composition of the immunological synapse between CTL and target cells have recently been described at different peptide concentrations (41), resulting in different signaling pathways and activation thresholds in individual CTL.

It appears, therefore, that the "consensus optimization" of the NY–ESO-$1_{157–165}$ F-pocket anchor side chain to valine can achieve increased T cell stimulation by augmenting the peptide affinity to A2, while maintaining, and in at least one case enhancing TCR recognition by decreasing the dissociation rate constant for TCR binding. Although the enhanced stability of the A2–ESO 9V variant was expected, our combined structural and functional analysis underscores the importance of also assessing the indirect effect of anchor residue changes on the TCR recognition surface.

The central role of the MW peg in our complex structures is consistent with results obtained for an alanine scan of the ESO 9C peptide using NY–ESO-$1_{157–165}$–specific T cell lines (42). A recent paper by Webb and colleagues confirmed the presence of this feature in the isolated A2–ESO 9C structure (43). We have extended the analysis of Webb et al. by determining a high resolution structure (1.5 Å) of unliganded A2 molecules loaded with the NY–ESO-$1_{157–165}$ peptide analogue bearing a leucine at position 165 (A2–ESO 9L), which demonstrates that the overall structure of the ESO 9L epitope in A2 is similar to the structure of the A2–ESO 9V and A2–ESO 9C complexes (unpublished data). It is of interest, however, that for isolated structures the MW side chains are more disordered than in the TCR complexes, consistent with the possibility that binding of the 1G4 TCR stabilizes the MW peg. Our study has primarily focused on TCR binding in assessing factors to be considered when engineering peptide analogs. However, CD8 binding to class I molecules is important for stabilizing the interaction between low affinity TCR and class I molecules (44) and for controlling the dynamics of CTL activation and immunological synapse formation (45). Consistent with these findings, we have shown that higher affinity recognition of the ESO 9V peptide by the 1G4 TCR is less CD8 dependent than recognition of the ESO 9C peptide. This alteration in CD8 dependency does not require any change in TCR docking orientation and therefore does not conform to the model suggested by Buslepp and colleagues (46).

The amount of signal that T cells receive by interacting with APCs is determined by several parameters including the concentration of pMHC complex (class I–peptide binding affinity) and the duration of the interaction between T cells and APCs (TCR binding affinity). From this concept it follows that the success of vaccine strategies will be dependent on our ability to fine tune several parameters to induce strong T cell expansions. The use of superagonist analogs in clinical applications provides an opportunity to address some of the shortcomings of current vaccination strategies, as it has been shown that peptide analogs can induce stronger responses than wild-type peptides in vivo (36–40). Peptide analogs are particularly relevant in the context of recombinant viral vector vaccination strategies, because immunodominance of viral vector–specific responses often impairs their ability to elicit immune responses specific for recombinant epitopes. It is possible that the low frequency of recombinant epitope–specific CTL responses may be due to competition from immunodominant viral epitope–specific responses, underscoring the need for engineering high-affinity peptide analogs for recombinant virus vaccine approaches.

In conclusion, our results highlight the indirect effects of anchor residue substitutions on TCR binding, effects that are of substantial significance for the rational optimization of vaccination strategies. The sensitivity of TCR recognition can extend to detect differences in buried anchor side chains, resulting in altered TCR binding kinetics and different levels of activation signals. Our results suggest the importance of incorporating structural data into the process of identifying candidate superagonist peptide analogs. Identification of highly antigenic NY–ESO-1 peptide analogs is of importance for the development of vaccines capable of expanding NY–ESO-1–specific CTL in cancer patients. Phase 1 clinical trials using NY–ESO-1 synthetic protein, peptides and recombinant viruses are already in progress aimed at eliciting

tumor-specific T cell responses. The use of the NY–ESO-1 9V analogue should be considered in future clinical trials, because it could result in a more efficient induction of NY–ESO-$1_{157–165}$–specific CTL in cancer patients.

MATERIALS AND METHODS

pMHC production. Residues 1–278 of the A2 heavy chain with the COOH-terminal BirA tag were expressed in *Escherichia coli* as inclusion bodies and refolded and purified with the NY–ESO-1 peptides SLLMWITQC or SLLMWITQV and β_2 m as described previously (for example see reference 47).

Expression and purification of the 1G4 NY–ESO-1 TCR. The 1G4 TCR was refolded and purified from *E. coli* derived inclusion bodies as described in reference 6.

Crystallization and x-ray diffraction data collection. Initial crystallization screens for the 1G4 TCR (10 mg/ml), 1G4–A2-ESO 9C or 1G4–A2-ESO 9V complexes (1:1 TCR–pMHC ratio at 10 mg/ml) used 100 nl + 100 nl drops dispensed by a Cartesian Technology Microsys MIC4000 (using Greiner 96-well protein crystallization plates), were stored in a automated vault and imaged with Veeco imaging systems. All crystallizations were done by the sitting drop vapor diffusion technique. Crystals of the isolated 1G4 TCR were grown at room temperature (21°C) from 2 μl + 2 μl protein + mother liquor (0.2 M sodium nitrate, 20% PEG 3350, pH 6.8) to dimensions of 180 μm × 130 μm × 70 μm. Crystals of the 1G4-A2-ESO 9C and 1G4-A2-ESO 9V complexes were grown at room temperature (21°C) from 2 μl + 2 μl protein + mother liquor (0.2 M potassium sodium tartarate tetrahydrate, 20% PEG 3350, pH 7.2) to dimensions of ~130 μm × 80 μm × 70 μm.

Crystals were cryoprotected in reservoir solutions containing 10 and 20% glycerol; they were then flash-cooled, and maintained at 100 K, using a cryostream (Oxford Cryosystems). High-resolution data sets (1.4 Å for the 1G4 TCR, 1.9 Å for the 1G4–A2-ESO 9C complex and 1.7 Å for the 1G4–A2-ESO 9V complex) were collected at station ID14 EH2 of the European Synchrotron Radiation Facility (ESRF, Grenoble, France) with an Area Detector Systems Corporation Quantum 4 CCD detector. The 1G4–A2-ESO 9C and the 1G4–A2–ESO 9V complex crystals belonged to space group $P2_1$. Data were auto-indexed and integrated with the program DENZO (48), and scaled with the program SCALEPACK (48; Table I).

Crystal structure determination, refinement, and analysis. The structures of the 1G4 TCR, 1G4–A2-ESO 9C, and the 1G4–A2-ESO 9V complexes were determined by molecular replacement with the program EPMR (49). For the two pMHC–TCR complexes, initial solutions were obtained for the HLA-A2 heavy chain, and β_2M followed by a second round of molecular replacement with the A6 TCR used as a search probe while the A2 solution was kept fixed. The 1G4 molecular replacement was solved with the A6 TCR in a single round of molecular replacement. The program SWISS-MODEL (www.expasy.org/swissmod/SWISS-MODEL.html) was used to replace the A6 TCR sequence with that of 1G4 before refinement.

Using CNS (50), the models were refined as rigid body domains (α1 and α2, α3, β_2M, peptide, Vα, Vβ, Cα, and Cβ for the complexes and the Vα, Vβ, Cα, and Cβ TCR domains for the 1G4 data). Subsequent minimization procedures included positional refinement, simulated annealing and restrained individual *B* factor refinement with bulk solvent correction and overall anisotropic *B* factor scaling. Manual refitting of the models was done with the interactive graphics program O (51), and water molecules were added at the last stages of refinement on the basis of peaks that were at least 3.0σ in height in $F_{obs} - F_{calc}$ electron density maps. The CDR loops of the isolated TCR showed significantly higher B factors than when complexed with pMHC, but the electron density was of sufficient quality to allow positioning of a single dominant main chain conformation for all of these loops.

We assessed the stereochemistry of the refined structures with the program PROCHECK (52). Surface complementarity calculations were done with the CCP4 program Sc (53; probe size 1.7 Å). To allow comparison of similar S_c values between structures it was necessary to estimate the standard uncertainty in atomic positions in the structures and how this translates to uncertainty in S_c value. For the 1G4–A2-ESO 9C complex (the lowest resolution structure) the standard uncertainty in atomic positions derived by Refmac (54) using the R_{free} was 0.148 Å. By running Sc 100 times on an ensemble of structures for this complex with the x, y, and z coordinates of each atom randomly perturbed using a Gaussian distribution of standard deviation 0.148 Å, we estimate the standard uncertainty in S_c to be 0.017. Thus, although the difference in S_c values for the two complexes is small, we believe it to be significant. Solvent accessibility calculations were done with Naccess (http://wolf.bms.umist.ac.uk/naccess/; probe size 1.4 Å). Graphical representations of the structure were prepared using programs Bobscript (55) and CSC Chemdraw (Cambridge Scientific Computing, Inc.).

Surface plasmon resonance. Surface plasmon resonance experiments were performed by using a Biacore3000 (Biacore). Biotinylated soluble HLA (ligand) was immobilized on Streptavidin-coated CM5 chip (Biacore) at the level of 1,000 RU (response units) per flow cell. Equilibrium binding was measured at the flow rate of 5 μl/min, starting from the lowest analyte concentration. The data points were plotted using Origin software. K_d values were calculated using the standard hyperbolic model fitting kinetics experiments. Kinetics of TCR–pMHC interactions was measured at 30 μl/min. The curves were then fitted using a simultaneous k_{on}/k_{off} fitting model (Bioevaluation software; Biacore).

MHC class I assembly assay. This assay was performed as previously described (31).

Flow cytometry. 3×10^4 T2 cells were pulsed with different concentrations of peptides for 2 h at 37°C. Cells were incubated with 40 μg/ml biotinylated Fab antibodies for 30 min at 4°C and visualized by Streptavidin-conjugated R-PE (Sigma-Aldrich) for 20 min at room temperature.

Confocal microscopy analysis. T2 target cells were pulsed with 1 μM, 100 nM, 10 nM, 5 nM, and 1 nM of either ESO 9C or ESO 9V peptide for 1 h at 37°C and washed twice in PBS. 1G4 CTL and T2 cells were washed in PBS and each cell pellet was resuspended to a final concentration of 5×10^5 cells/ml in RPMI. 1G4 CTL and target were mixed 1:1, left for 5 min in suspension, and the plated on glass multiwell slides and incubated for 30 min at 37°C. Cells were fixed in 100% methanol precooled to −20°C, washed in PBS, and blocked in PBS, 2% BSA (Sigma-Aldrich). The slides were mounted in PBS containing 90% glycerol and 2.5% DABCO. Samples were examined using a Bio-Rad Radiance 2000 MP laser scanning microscope and the conjugation rate and granule polarization were quantified using an Axioplan 2 epifluorescent microscope (Zeiss).

Live cell video microscopy. 2×10^4 1G4 CTL were incubated with 60 nM lysotracker green DND-26 (Molecular Probes) for 1 h at 37°C in RPMI, 5% human serum, and washed once in PBS and resuspended in 100 ml RPMI without phenol red, 5% human serum, 1 mM Hepes. T2 target cells were pulsed with 1 μM of either ESO 9C peptide or ESO 9V peptide for 1 h at 37°C and washed twice in PBS. 2×10^4 target cells were allowed to adhere on a glass coverslip mounted in a temperature-controlled chamber for 10 min at 37°C in RPMI without serum, without phenol red plus Hepes. Lysotracker green DND-26–labeled 1G4 NY–ESO-$1_{157–165}$ CTL were added to the T2 cells in the chamber. Sequential confocal images were acquired every 20 s.

CD8-independent ELISA assays for soluble cytokines. 1G4 CTL and pulsed B cell targets were incubated at 37°C for 4 h at an effector–target ratio of 1:1. After 4 h the supernatant was harvested and assayed for MIP-1β and IFN-γ by ELISA (R&D Systems). Standard deviation from the mean of two duplicate assays is shown.

Vaccination of A2K^b mice and ex vivo tetramer staining. A2K^b transgenic mice were vaccinated using a DNA-prime/recombinant vaccinia virus–boost strategy (56). Mice were injected intramuscularly with 50 μg plasmid DNA encoding either ESO 9V or ESO 9C peptide followed by intravenous injection with 5×10^6 plaque forming units recombinant vaccinia virus containing the same antigens on day 10. 10 d after injection, fresh PBL were isolated from blood taken from the tail vein using red cell lysis buffer (Invitrogen). A2K^b tetramer for ex vivo staining were synthesized as previously described (57). Approval of care and use of animals was obtained from the Clinical Medicine Ethical Review Committee (University of Oxford, Oxford, UK) and by the UK Home Office.

Ex-vivo IFN-γ ELISPOT assay. ELISPOT analysis for mouse IFN-γ secretion was performed with cells incubated overnight according to the protocol provided by the manufacturer (Mabtech). Mice splenocytes were generated using the method described above and rested in RPMI supplemented with 10% FCS at 4°C overnight.

In the experiment shown in Fig. 6 D, ESO 9C peptide was treated with 20 mM TCEP at room temperature for 1 h before being added to the wells at the final concentration of 200 μM.

Accession numbers. Atomic coordinates and structure factor amplitudes for the 1G4 TCR–ESO 9C–A2 complex, 1G4 TCR–ESO 9V–A2 complex, and the 1G4 TCR have been deposited in the Protein Data Bank under accession numbers 2BNR, 2BNQ, and 2BNU, respectively.

Online supplemental materials. For surface plasmon resonance, the antibody binding assay shown in Fig. S1, 10 serial dilutions in duplicates of BB7.2 and BBM.1 were made. For live cell video microscopy (Videos 1 and 2) a Nikon TE300 microscope attached to a Bio-Rad Radiance 200 MP laser scanning microscope was used with a 488-nm laser for epifluorescence and Nomarski differential interference contrast for transmitted light. The images were processed using MetaMorph version 4.5 software. Online supplemental material is available at http://www.jem.org/cgi/content/full/jem.20042323/DC1.

The authors wish to thank Dawn Shepherd, Ian Hermans, Uzi Gileadi, Jonathan Silk, Michael Palmowski, Fareed Mirza, and David Stuart for helpful discussions and assistance. We are also grateful to Karl Harlos and the staff of the ESRF and EMBL in Grenoble for assistance with X-ray data collection. We acknowledge use of crystallization facilities provided by the MRC-funded Oxford Protein Production Facility and The European Commission Integrated Programme (SPINE, Grant code QLRT-2001-00988).

E.Y. Jones is a Cancer Research UK Principal Research Fellow. This work was funded by Cancer Research UK (C399-A2291), the US Cancer Research Institute, the UK Medical Research Council, and National Translational Cancer Research Network. G. Held was supported by the German Research Foundation. G. Griffiths is funded by the Wellcome Trust.

The authors have no conflicting financial interests.

Submitted: 12 November 2004
Accepted: 16 February 2005

REFERENCES

1. Rosenberg, S.A., J.C. Yang, D.J. Schwartzentruber, P. Hwu, F.M. Marincola, S.L. Topalian, N.P. Restifo, M.E. Dudley, S.L. Schwarz, P.J. Spiess, et al. 1998. Immunologic and therapeutic evaluation of a synthetic peptide vaccine for the treatment of patients with metastatic melanoma. *Nat. Med.* 4:321–327.
2. Apostolopoulos, V., M. Yu, I.F. McKenzie, and I.A. Wilson. 2000. Structural implications for the design of molecular vaccines. *Curr. Opin. Mol. Ther.* 2:29–36.
3. Apostolopoulos, V., M. Yu, A. Corper, L. Teyton, G. Pietersz, I. McKenzie, I. Wilson, and M. Plebanski. 2002. Crystal structure of a non-canonical low-affinity peptide complexed with MHC class I: a new approach for vaccine design. *J. Mol. Biol.* 318:1293–1305.
4. Madden, D.R. 1995. The three-dimensional structure of peptide-MHC complexes. *Annu. Rev. Immunol.* 13:587–622.
5. Rudolph, M.G., J.G. Luz, and I.A. Wilson. 2002. Structural and thermodynamic correlates of T cell signalling. *Annu. Rev. Biophys. Biomol. Struct.* 31:121–149.
6. Boulter, J.M., M. Glick, P.T. Todorov, E. Baston, M. Sami, P. Rizkallah, and B.K. Jakobsen. 2003. Stable, soluble T-cell receptor molecules for crystallization and therapeutics. *Protein Eng.* 16:707–711.
7. Reid, S.W., S. McAdam, K.J. Smith, P. Klenerman, C.A. O'Callaghan, K. Harlos, B.K. Jakobsen, A.J. McMichael, J.I. Bell, D.I. Stuart, and E.Y. Jones. 1996. Antagonist HIV-1 Gag peptides induce structural changes in HLA B8. *J. Exp. Med.* 184:2279–2286.
8. Velloso, L.M., J. Michaelsson, H.G. Ljunggren, G. Schneider, and A. Achour. 2004. Determination of structural principles underlying three different modes of lymphocytic choriomeningitis virus escape from CTL recognition. *J. Immunol.* 172:5504–5511.
9. Sharma, A.K., J.J. Kuhns, S. Yan, R.H. Friedline, B. Long, R. Tisch, and E.J. Collins. 2001. Class I major histocompatibility complex anchor substitutions alter the conformation of T cell receptor contacts. *J. Biol. Chem.* 276:21443–21449.
10. Degano, M., K.C. Garcia, V. Apostolopoulos, M.G. Rudolph, L. Teyton, and I.A. Wilson. 2000. A functional hot spot for antigen recognition in a superagonist TCR/MHC complex. *Immunity.* 12:251–261.
11. Ding, Y.H., B.M. Baker, D.N. Garboczi, W.E. Biddison, and D.C. Wiley. 1999. Four A6-TCR/peptide/HLA-A2 structures that generate very different T cell signals are nearly identical. *Immunity.* 11:45–56.
12. Luz, J.G., M. Huang, K.C. Garcia, M.G. Rudolph, V. Apostolopoulos, L. Teyton, and I.A. Wilson. 2002. Structural comparison of allogeneic and syngeneic T cell receptor-peptide-major histocompatibility complex complexes: a buried alloreactive mutation subtly alters peptide presentation substantially increasing Vβ interactions. *J. Exp. Med.* 195: 1175–1186.
13. Garcia, K.C., M.D. Tallquist, L.R. Pease, A. Brunmark, C.A. Scott, M. Degano, E.A. Stura, P.A. Peterson, I.A. Wilson, and L. Teyton. 1997. Alphabeta T cell receptor interactions with syngeneic and allogeneic ligands: affinity measurements and crystallization. *Proc. Natl. Acad. Sci. USA.* 94:13838–13843.
14. Kersh, G.J., and P.M. Allen. 1996. Structural basis for T cell recognition of altered peptide ligands: a single T cell receptor can productively recognize a large continuum of related ligands. *J. Exp. Med.* 184:1259–1268.
15. Davis, M.M., M. Krogsgaard, J.B. Huppa, C. Sumen, M.A. Purbhoo, D.J. Irvine, L.C. Wu, and L. Ehrlich. 2003. Dynamics of cell surface molecules during T cell recognition. *Annu. Rev. Biochem.* 72:717–742.
16. Van der Merwe, P.A., and S.J. Davis. 2003. Molecular interactions mediating T cell antigen recognition. *Annu. Rev. Immunol.* 21:659–684.
17. Chen, Y.T., M.J. Scanlan, U. Sahin, O. Tureci, A.O. Gure, S. Tsang, B. Williamson, E. Stockert, M. Pfreundschuh, and L.J. Old. 1997. A testicular antigen aberrantly expressed in human cancers detected by autologous antibody screening. *Proc. Natl. Acad. Sci. USA.* 94:1914–1918.
18. Jager, E., Y.T. Chen, J.W. Drijfhout, J. Karbach, M. Ringhoffer, D. Jager, M. Arand, H. Wada, Y. Noguchi, E. Stockert, et al. 1998. Simultaneous humoral and cellular immune response against cancer-testis antigen NY–ESO-1: definition of human histocompatibility leukocyte antigen (HLA)-A2-binding peptide epitopes. *J. Exp. Med.* 187:265–270.
19. Chen, J.L., P.R. Dunbar, U. Gileadi, E. Jager, S. Gnjatic, Y. Nagata, E. Stockert, D.L. Panicali, Y.T. Chen, A. Knuth, et al. 2000. Identification of NY-ESO-1 peptide analogues capable of improved stimulation of tumor-reactive CTL. *J. Immunol.* 165:948–955.
20. Stewart-Jones, G.B., A.J. McMichael, J.I. Bell, D.I. Stuart, and E.Y. Jones. 2003. A structural basis for immunodominant human T cell receptor recognition. *Nat. Immunol.* 4:657–663.
21. Buslepp, J., S. Kerry, D. Loftus, J. Frelinger, E. Appella, and E. Collins. 2003. High affinity xenoreactive TCR:MHC interaction recruits CD8 in absence of binding to MHC. *J. Immunol.* 170:373–383.
22. Garboczi, D.N., P. Ghosh, U. Utz, Q.R. Fan, W.E. Biddison, and D.C. Wiley. 1996. Structure of the complex between human T-cell receptor, viral peptide and HLA-A2. *Nature.* 384:134–141.
23. Garcia, K.C., M. Degano, R.L. Stanfield, A. Brunmark, M.R. Jackson,

P.A. Peterson, L. Teyton, and I.A. Wilson. 1996. An alphabeta T cell receptor structure at 2.5 A and its orientation in the TCR-MHC complex. *Science*. 274:209–219.
24. Reiser, J.B., C. Darnault, A. Guimezanes, C. Gregoire, T. Mosser, A.M. Schmitt-Verhulst, J.C. Fontecilla-Camps, B. Malissen, D. Housset, and G. Mazza. 2000. Crystal structure of a T cell receptor bound to an allogeneic MHC molecule. *Nat. Immunol.* 1:291–297.
25. Garcia, K.C., M. Degano, L.R. Pease, M. Huang, P.A. Peterson, L. Teyton, and I.A. Wilson. 1998. Structural basis of plasticity in T cell receptor recognition of a self peptide-MHC antigen. *Science*. 279: 1166–1172.
26. Hare, B.J., D.F. Wyss, M.S. Osburne, P.S. Kern, E.L. Reinherz, and G. Wagner. 1999. Structure, specificity and CDR mobility of a class II restricted single-chain T-cell receptor. *Nat. Struct. Biol.* 6:574–581.
27. Reiser, J.B., C. Gregoire, C. Darnault, T. Mosser, A. Guimezanes, A.M. Schmitt-Verhulst, J.C. Fontecilla-Camps, G. Mazza, B. Malissen, and D. Housset. 2002. A T cell receptor CDR3beta loop undergoes conformational changes of unprecedented magnitude upon binding to a peptide/MHC class I complex. *Immunity*. 16:345–354.
28. Reiser, J.B., C. Darnault, C. Gregoire, T. Mosser, G. Mazza, A. Kearney, P.A. van der Merwe, J.C. Fontecilla-Camps, D. Housset, and B. Malissen. 2003. CDR3 loop flexibility contributes to the degeneracy of TCR recognition. *Nat. Immunol.* 4:241–247.
29. Kjer-Nielsen, L., C.S. Clements, A.W. Purcell, A.G. Brooks, J.C. Whisstock, S.R. Burrows, J. McCluskey, and J. Rossjohn. 2003. A structural basis for the selection of dominant alphabeta T cell receptors in antiviral immunity. *Immunity*. 18:53–64.
30. Rammensee, H., K. Falk, and O. Rotzschke. 1993. Peptides naturally presented by MHC class I molecules. *Annu. Rev. Immunol.* 11:213–244.
31. Townsend, A., T. Elliott, V. Cerundolo, L. Foster, B. Barber, and A. Tse. 1990. Assembly of MHC class I molecules analyzed in vitro. *Cell*. 62:285–295.
32. Held, G., M. Matsuo, M. Epel, S. Gnjatic, G. Ritter, Y.S. Lee, T.Y. Tai, C.J. Cohen, L.J. Old, M. Pfreundschuh, Y. Reiter, H.R. Hoogenboom, and C. Renner. 2004. Dissecting cytotoxic T cell responses towards the NY-ESO-1 protein by peptide/MHC-specific antibody fragments. *Eur. J. of Immunol.* 34: 2919–2929.
33. Stinchcombe, J.C., G. Bossi, S. Booth, and G.M. Griffiths. 2001. The immunological synapse of CTL contains a secretory domain and membrane bridges. *Immunity*. 15:751–761.
34. Chen, W., J.W. Yewdell, R.L. Levine, and J.R. Bennink. 1999. Modification of cysteine residues in vitro and in vivo affects the immunogenicity and antigenicity of major histocompatibility complex class I-restricted viral determinants. *J. Exp. Med.* 189:1757–1764.
35. Wang, B., A. Sharma, R. Maile, M. Saad, E. Collins, and J. Frelinger. 2002. Peptidic termini play a significant role in TCR recognition. *J. Immunol.* 169:3137–3145.
36. Bakker, A.B., S.H. van der Burg, R.J. Huijbens, J.W. Drijfhout, C.J. Melief, G.J. Adema, and C.G. Figdor. 1997. Analogues of CTL epitopes with improved MHC class-I binding capacity elicit anti-melanoma CTL recognizing the wild-type epitope. *Int. J. Cancer.* 70:302–309.
37. Dyall, R., W.B. Bowne, L.W. Weber, J. LeMaoult, P. Szabo, Y. Moroi, G. Piskun, J.J. Lewis, A.N. Houghton, and J. Nikolic-Zugic. 1998. Heteroclitic immunization induces tumor immunity. *J. Exp. Med.* 188:1553–1561.
38. Overwijk, W.W., A. Tsung, K.R. Irvine, M.R. Parkhurst, T.J. Goletz, K. Tsung, M.W. Carroll, C. Liu, B. Moss, S.A. Rosenberg, and N.P. Restifo. 1998. gp100/pmel 17 is a murine tumor rejection antigen: induction of "self"-reactive, tumoricidal T cells using high-affinity, altered peptide ligand. *J. Exp. Med.* 188:277–286.
39. Valmori, D., J.F. Fonteneau, S. Valitutti, N. Gervois, R. Dunbar, D. Lienard, D. Rimoldi, V. Cerundolo, F. Jotereau, J.C. Cerottini, et al. 1999. Optimal activation of tumor-reactive T cells by selected antigenic peptide analogues. *Int. Immunol.* 11:1971–1980.
40. Slansky, J.E., F.M. Rattis, L.F. Boyd, T. Fahmy, E.M. Jaffee, J.P. Schneck, D.H. Margulies, and D.M. Pardoll. 2000. Enhanced antigen-specific antitumor immunity with altered peptide ligands that stabilize the MHC-peptide-TCR complex. *Immunity*. 13:529–538.
41. Faroudi, M., C. Utzny, M. Salio, V. Cerundolo, M. Guiraud, S. Muller, and S. Valitutti. 2003. Lytic versus stimulatory synapse in cytotoxic T lymphocyte/target cell interaction: manifestation of a dual activation threshold. *Proc. Natl. Acad. Sci. USA*. 100:14145–14150.
42. Romero, P., V. Dutoit, V. Rubio-Godoy, D. Lienard, D. Speiser, P. Guillaume, K. Servis, D. Rimoldi, J.C. Cerottini, and D. Valmori. 2001. CD8+ T-cell response to NY-ESO-1: relative antigenicity and in vitro immunogenicity of natural and analogue sequences. *Clin. Cancer Res.* 7:766s–772s.
43. Webb, A.I., M.A. Dunstone, W. Chen, M.I. Aguilar, Q. Chen, H. Jackson, L. Chang, L. Kjer-Nielsen, T. Beddoe, J. McCluskey, et al. 2004. Functional and structural characteristics of NY-ESO-1 related HLA-A2 restricted epitopes and the design of a novel immunogenic analogue. *J. Biol. Chem.* 279:23438–23446.
44. Garcia, K.C., C.A. Scott, A. Brunmark, F.R. Carbone, P.A. Peterson, I.A. Wilson, and L. Teyton. 1996. CD8 enhances formation of stable T-cell receptor/MHC class I molecule complexes. *Nature*. 384:577–581.
45. Purbhoo, M.A., D.J. Irvine, J.B. Huppa, and M.M. Davis. 2004. T cell killing does not require the formation of a stable mature immunological synapse. *Nat. Immunol.* 5:524–530.
46. Buslepp, J., H. Wang, W.E. Biddison, E. Appella, and E.J. Collins. 2003. A correlation between TCR Valpha docking on MHC and CD8 dependence: implications for T cell selection. *Immunity*. 19:595–606.
47. Madden, D.R., D.N. Garboczi, and D.C. Wiley. 1993. The antigenic identity of peptide-MHC complexes: a comparison of the conformations of five viral peptides presented by HLA-A2. *Cell*. 75:693–708.
48. Otwinowski, Z., and W. Minor. 1997. Processing of X-ray diffraction data collected in oscillation mode. *Methods Enzymol.* 276:307–326.
49. Kissinger, C.R., D.K. Gehlhaar, and D.B. Fogel. 1999. Rapid automated molecular replacement by evolutionary search. *Acta Crystallogr. D Biol. Crystallogr.* 55:484–491.
50. Brunger, A.T., P.D. Adams, G.M. Clore, W.L. DeLano, P. Gros, R.W. Grosse-Kunstleve, J.S. Jiang, J. Kuszewski, M. Nilges, N.S. Pannu, et al. 1998. Crystallography & NMR system: A new software suite for macromolecular structure determination. *Acta Crystallogr. D Biol. Crystallogr.* 54:905–921.
51. Jones, T.A., J.Y. Zou, S.W. Cowan, and Kjeldgaard. 1991. Improved methods for building protein models in electron density maps and the location of errors in these models. *Acta Crystallogr. A* 47:110-119.
52. Laskowski, R.A., M. MacArthur, D. Moss, and J. Thornton. 1993. PROCHECK: a program to check the stereochemical quality of protein structures. *J. Appl. Cryst.* 26:283–291.
53. Lawrence, M.C., and P.M. Colman. 1993. Shape complementarity at protein/protein interfaces. *J. Mol. Biol.* 234:946–950.
54. Murshudov, G.N., A.A. Vagin, and E.J. Dodson. 1997. Refinement of macromolecular structures by the maximum-likelihood method. *Acta Crystallogr. D Biol. Crystallogr.* 53:240–255.
55. Esnouf, R.M. 1999. Further additions to MolScript version 1.4, including reading and contouring of electron-density maps. *Acta Crystallogr. D Biol. Crystallogr.* 55:938–940.
56. Palmowski, M., M. Salio, R.P. Dunbar, and V. Cerundolo. 2002. The use of HLA class I tetramers to design a vaccination strategy for melanoma patients. *Immunol. Rev.* 188:155–163.
57. Choi, E.M., M. Palmowski, J. Chen, and V. Cerundolo. 2002. The use of chimeric A2K(b) tetramers to monitor HLA A2 immune responses in HLA A2 transgenic mice. *J. Immunol. Methods*. 268:35–41.